DROPLET GROWTH KINETICS ON SUPERHYDROPHOBIC SURFACES AND FUTURE WORK ON COMBATING CRYOGENIC SURFACE CONTAMINATION

BY

JAMES CARPENTER

THESIS

Submitted in partial fulfillment of the requirements
for the degree of Master of Science in Mechanical Engineering
in the Graduate College of the
University of Illinois at Urbana-Champaign, 2018

Urbana, Illinois

Adviser:

Assistant Professor Nenad Miljkovic

ABSTRACT

In the first part of this thesis, I discuss my work on droplet growth kinetics during dropwise condensation. Accurate heat transfer predictions during dropwise condensation depend on the growth rates of the condensing droplets. This includes both the heat transfer rate during droplet growth as well as following droplet sweeping—where large droplets sweep away other droplets on an inclined surface. Droplet growth rates on a given surface primarily depend on background vapor pressure and the extent of wall subcooling. Here, I report that larger droplets affect the growth rates of nearby smaller droplets during dropwise condensation on superhydrophobic aluminum surfaces. In large systems, neglecting this influence is less of a concern as the error will largely be contained in the uncertainty of the heat transfer rate prediction. However, in smaller phase-change heat transfer systems, like those currently being explored to cool MEMS/NEMS devices, accurate predictions of droplet growth rates are crucial. In this work, using high-angle environmental scanning electron microscopy (ESEM), I report visualizations of the effect that larger droplets have on the growth rates of nearby smaller droplets. Furthermore, I also hypothesize the underlying mechanism behind this phenomenon and discuss my ongoing work to validate this hypothesis.

In the second part of this thesis, I propose a project to use functionalized surfaces to combat contamination of low-emissivity cryogenic surfaces. Future crewed space missions require high capacity cryocoolers for zero boil-off (ZBO) systems. Due to parasitic heat loads, cryocoolers have low efficiency, making approaches to limiting these loads highly desired. Water cryodepositing onto low-emissivity cryogenic surfaces results in high parasitic radiative loads. In this project, I propose a method for combating this load increase. Specifically, I propose to use a functionalized

(biphilic) surface to getter water onto a small percentage (< 5 %) of the cryogenic surface, thus maintaining an overall low-emissivity. I aim to determine whether (1) the spatial control of water nucleation that the biphilic surface exhibits in non-cryogenic conditions extend to cryogenic conditions, (2) the biphilic surface maintains the low-emissivity of the cryogenic surface, and (3) the biphilic surface is durable in space-cryocooler applications. I discuss the preliminary considerations and objectives for this work, including the proposed fabrication and characterization process for the biphilic surfaces, as well as the proposed experimental apparatus to be used in conducting experiments.

ACKNOWLEDGEMENTS

I would like to thank my adviser, Dr. Nenad Miljkovic, who has taught me so much in my time here. I can say without reservation that any increase in my capacity as a scientist is due to his guidance. I would further like to thank all the members of the Energy Transport Research Lab who have entertained my countless questions and fleeting ideas about one thing or another; a special thanks to Alex Wu and Shreyas Chavan who have endured more than most.

I would also like to thank both the College of Engineering and Mechanical Science and Engineering Department at the University of Illinois at Urbana-Champaign for financial and academic support throughout my master's thesis work.

Finally, I am grateful to my mother, my father, and my brothers and sisters for believing in me throughout my academic and professional pursuits. I am truly fortunate to have a family that believes in me so absolutely.

TABLE OF CONTENTS

Part I: Droplet Growth Kinetics on Superhydrophobic Surfaces

1. INTRODUCTION

1.1. Dropwise Condensation

Heterogeneous condensation of water vapor occurs in a variety of natural phenomena.[1-3] It is also essential in a range of industrial applications, such as power generation,[4] water desalination,[5,6] thermal management,[7] and environmental control.[8] Dropwise condensation, where vapor condenses as droplets that partially wet the surface, has been established as a more efficient means of phase change heat transfer than filmwise condensation, where vapor condenses as a film and completely wets the surface. In fact, dropwise condensation enables 10-20 times greater heat transfer performance when compared to filmwise condensation.[9]

To achieve dropwise condensation the surface must have a low wettability. The wettability of a surface is governed by Young's equation:

$$cos\ \theta = \frac{\gamma_{sv} - \gamma_{sl}}{\gamma_{lv}} \tag{1-1}$$

which relates the equilibrium contact angle θ to the surface energies at the solid-vapor interface γ_{sv}, solid-liquid interface γ_{sl} and the liquid-vapor interface γ_{lv}. If $\gamma_{sv} > \gamma_{sl}$, then the right side of equation (1) is positive (surface energies are positive values), which means for $\cos\theta$ to be positive $\theta < 90^0$. When $\theta < 90^0$ the surface is deemed hydrophilic and the liquid "wets" the surface, and when $\theta > 90^0$ the surface is deemed hydrophobic and the surface is non-wetting or has low wettability. Superhydrophobicity is a special case of hydrophobicity, where $\theta > 150^0$. Because of contact angle hysteresis, the equilibrium contact angle lies between the advancing θ_a and receding θ_r contact angles, with both being measured using a microgoniometer.

Studies on condensing droplet morphology and growth dynamics have been conducted in the past. Rykaczewski et al. [10,11] found that sub-10 μm diameter droplets first form and grow with a constant base area until a critical contact angle is reached (130-150^o). The droplet base then expands in a discrete step-like fashion, decreasing the contact angle, then grows once again until the critical contact angle is reached, repeating the process up to four times. He further found that the droplet growth rate was faster during the constant-base stage than the constant-contact-angle stage. However, the effect that condensing droplets have on the growth rates of nearby condensing droplets has been neglected. Neglecting this effect may lead to inaccurate predictions of heat transfer rates in phase-change cooling applications. In this work, I aimed to bridge this gap by analyzing the growth rates of smaller droplets in close proximity to larger ones on superhydrophobic surfaces.

2. METHODS

2.1. Sample Preparation

Superhydrophobic ($\theta_a \approx 160^o$) aluminum specimens were fabricated using a straightforward chemical vapor deposition process.[12] First, 1in x 1in aluminum samples (6061, 0.83in thick) were cut in the machine shop. These samples were then cleaned ultrasonically in acetone for five minutes, then ethanol for an additional five minutes. The specimens were then dried using nitrogen gas (N_2). Afterwards, the specimens were submerged in hot water (90 ^{0}C) for one hour oxidizing the aluminum sample, forming Al_2O_3. During the oxidation process, a sharp cauliflower-like structure forms increasing the surface roughness of the specimens, rendering them superhydrophilic. The surface roughness is needed to attain superhydrophobicity ($\theta_a > 150^0$). Following hot water submersion, the surfaces were rinsed with DI water and dried with N_2.

To render the surfaces superhydrophobic, the samples were placed in a beaker covered with aluminum foil containing a Heptadecafluorodecyltrimethoxy-silane (HTMS)-Toluene (C_7H_8) solution. The entire beaker was then placed in an oven at 80 ^oC for three hours, which reduced the surface energy of the samples. See Figure 2-1 for an illustration of this process. The samples were then taken out of the oven and allowed to cool to room temperature, while still being covered by the aluminum foil.

2.2. Experimental Apparatus

To remove the effects of non-condensable gases (NCGs), we conducted droplet growth experiments in an environmental scanning electron microscope (ESEM; Versa 3D, FEI) that enabled observation of microscale water droplets at saturation vapor pressures of up to 4 kPa ± 0.2%. The removal of NCGs eliminates the dominant vapor diffusion resistance which enables the principal condensation physics governing droplet growth to dominate. Before the experiments, a gas scanning electron detector (GSED) and a Peltier stage were mounted inside the ESEM chamber. Each sample substrate was attached to a 5 mm thick copper sample holder with carbon conductive tape and then mounted on the Peltier stage to control the temperature of the sample surface. The chamber was closed and pumped down to high vacuum mode (<1 MPa) to remove any contaminants or NCGs present in the chamber. Before condensation, the pressure in the chamber was maintained at <100 Pa and the surface temperature was set at 2 ± 0.1 °C. Before condensing, the set temperature was maintained for >10 min to ensure the surface temperature reached equilibrium. Water vapor pressure in the chamber was gradually increased at 50 Pa/min until condensation appeared on the surface at saturation pressures ranging from 630 to 700 Pa. The camera inclination was set to 45^o to the surface in order to capture nucleation and growth dynamics of smaller droplets (< ~ 20 μm diameter) in the immediate vicinity (< ~50 μm) to the three phase

contact line of larger droplets (~ 200 μm diameter). Over the time interval of the experiment reported here, the chamber relative humidity (RH) and saturation pressure were carefully maintained at 86.8 % $\pm$ 0.1 % and 700 Pa $\pm$ 1 Pa, respectively. While we imaged in four second intervals, we only included every other image in Figure 2-2.

2.3. Figures

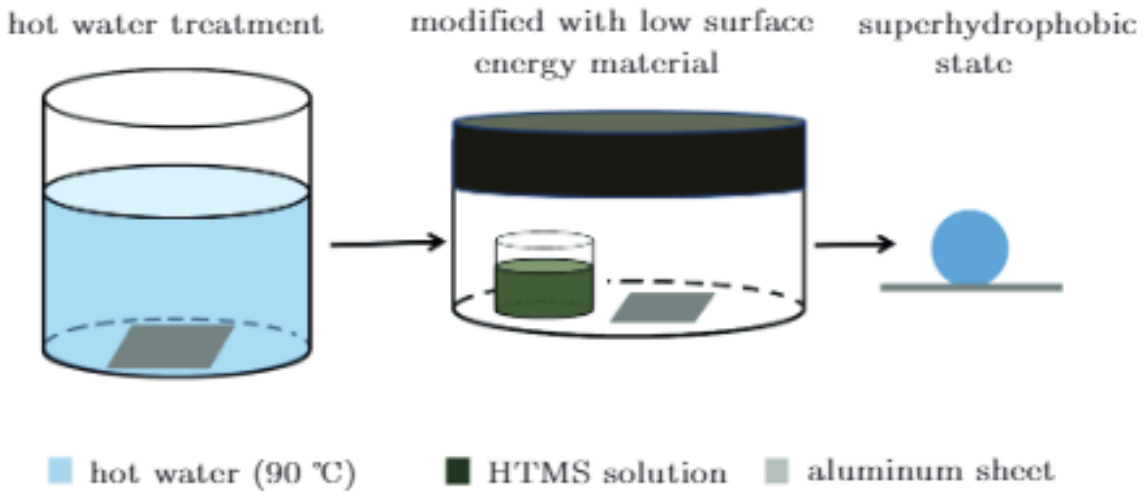

Figure 2-1. *Surface Functionalization Process.* An Illustration of the Surface Functionalization Process.[12]

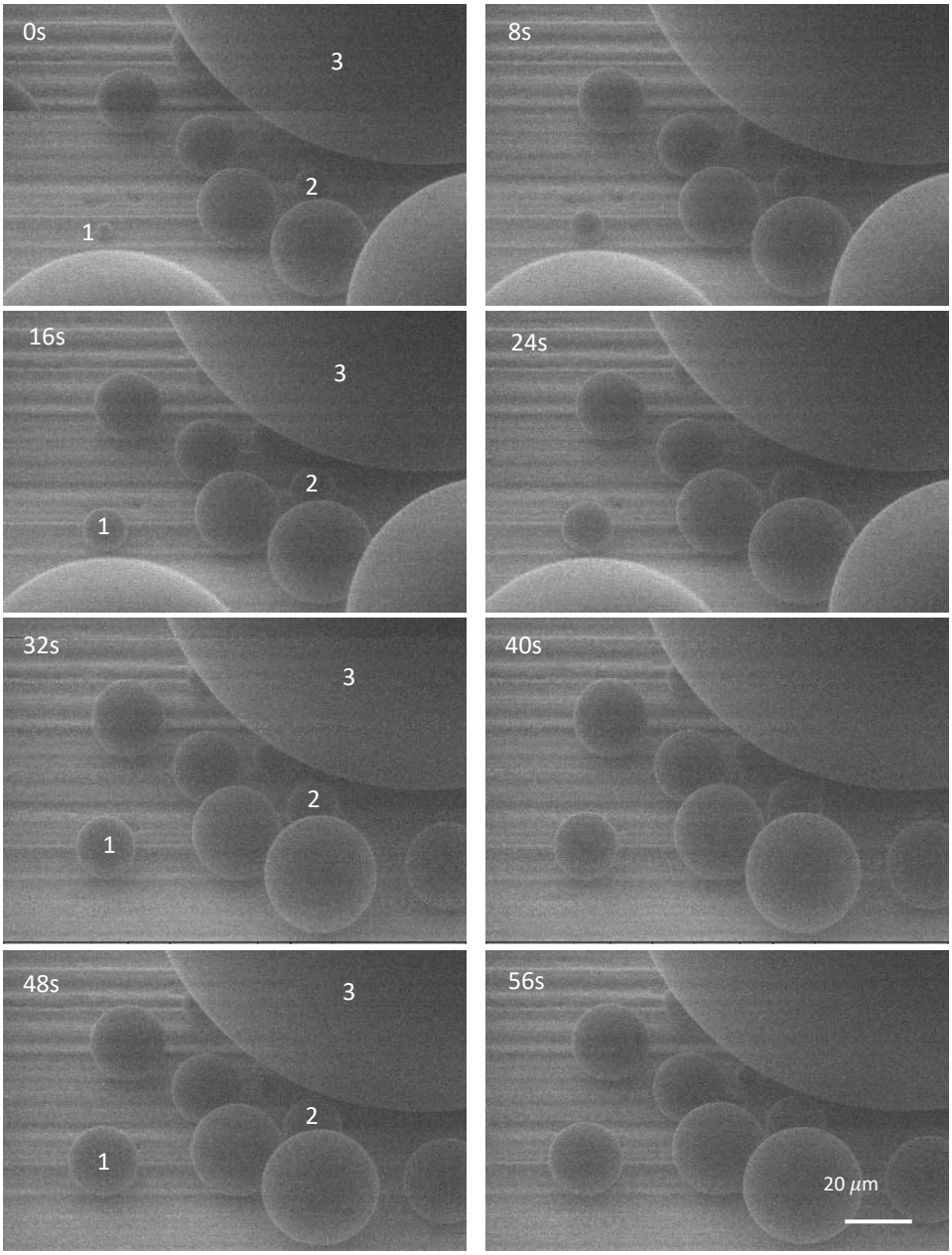

Figure 2-2. *Droplet Growth Images.* Droplets condensing on a superhydrophobic aluminum substrate. A time-stamp is included in the upper left corner of each image. Droplet 1 is the isolated droplet and grows much faster than droplet 2, which is closer to the three phase contact line of droplet 3.

3. RESULTS AND DISCUSSION

3.1. Results

Figure 2-2 shows a sequence of the images captured with the ESEM. As illustrated by the images, droplet 1 is ~ 80 μm from the three phase contact line of the larger droplet whereas droplet 2 is only ~ 35 μm from that point. The distances from the larger droplet were calculated using geometric relations and the radius of curvature of droplet 3. As seen in Figure 3-1, at every point in time, the growth rate of droplet 1 was greater than that of droplet 2. While these growth rates should not necessarily be the same over all diameter ranges, they should be the same over the same diameter ranges, since every measureable parameter affecting the growth rate is seemingly the same amongst the two droplets. Nevertheless, droplet 1 grows faster than droplet 2, so much faster that at ~20s it matches and surpasses the size of droplet 2 even though its initial size was less than half the initial size of droplet 2.

3.2. Discussion

One would expect the two droplets to grow at the same rate, though this is clearly not the case. Since the substrate temperature remains essentially constant, the local vapor supply must be being affected in some way. I posit that the larger droplet serves as a vapor "sink" if you will. The water molecules condensing into the larger droplet far outweigh the water molecules evaporating from the droplet. As a result, near the droplet, there exists a decrease in available vapor pressure that inhibits the growth rate of nearby smaller droplets.

Geometrically, one can imagine how the large size of the droplet could intercept a fraction of the water molecules that would have condensed within the smaller droplet had it been isolated. How big of a fraction would depend on the size of the respective droplets and the distance between their

respective centers. For a droplet on a surface, the probability that a vapor molecule will collide with it increases with increasing angle from the surface since molecules approaching at lower angles are more likely to be intercepted by surrounding droplets. This probability distribution is similar for all non-edge droplets on the surface, which is why most similarly-sized droplets grow at the same rate (i.e., they have the same vapor supply). However, a smaller droplet sufficiently close to a larger droplet has its probability distribution altered since the larger droplet intercepts vapor molecules approaching at higher angles, molecules that would have collided and condensed in the smaller droplets. This results in smaller growth rates for these droplets. In other words, there exists a region surrounding the larger droplet, a "sphere of influence," where a vapor pressure gradient exists that influences the growth rates of all smaller droplets residing there. I propose that the effect of this pressure gradient on the growth rate of smaller droplets can be determined geometrically based on the fraction of molecules that would have collided with the droplet had it been isolated, using the projected shadow of the larger droplet to aid in this determination. Future work is underway using kinetic theory calculations of rarefied vapor flow in the geometric conditions encountered here to validate these assertions.

3.3. Conclusion

In this work, I provided visualizations of micro-scale droplets condensing on a superhydrophobic aluminum surface. The images showed that the growth rates of condensing droplets are affected by their proximity to other larger droplets. I further provided a hypothesis on the physics underlying this phenomenon, a hypothesis that is currently being validated. Correct predictions of droplet growth rates become more crucial the smaller the scale of the system. Therefore, I believe this work will be most useful when predicting heat transfer rates in future MEMS/NEMS phase-change cooling applications.

3.4. Figures

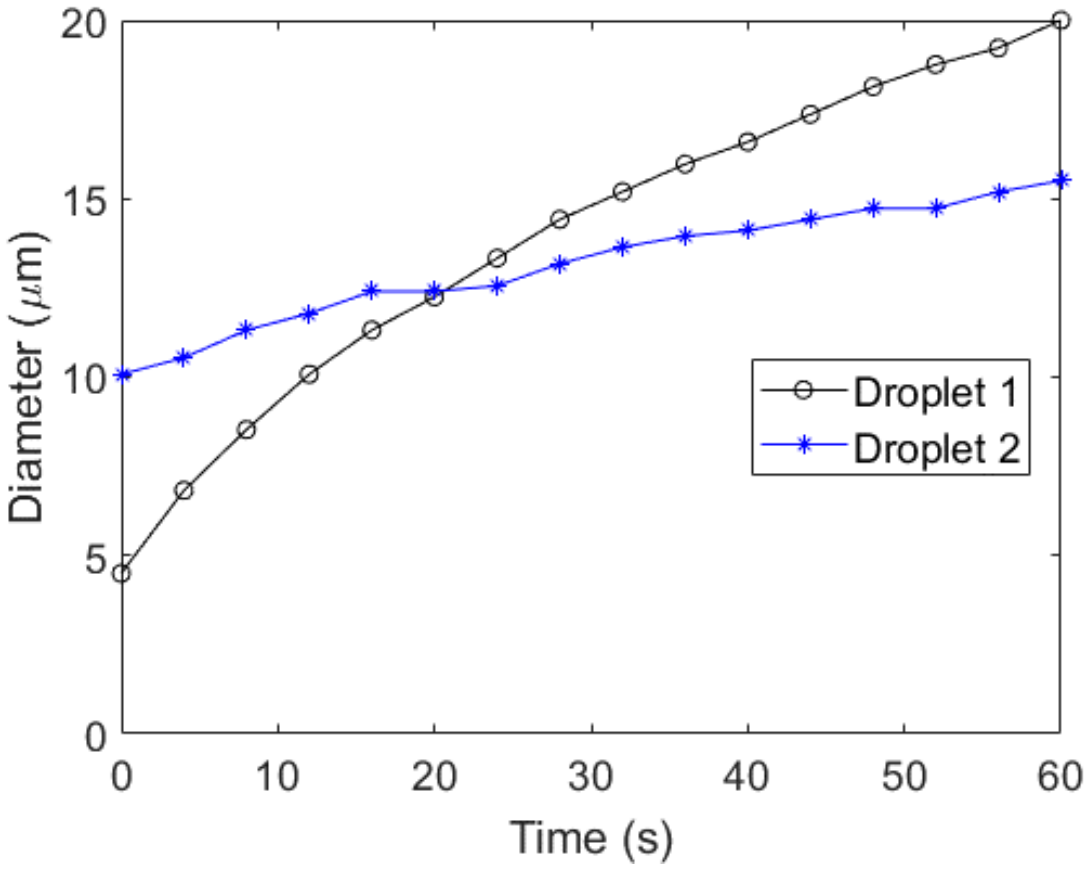

Figure 3-1. *Droplet Growth Rate Comparison.* Comparison between the two droplets growth rates. Note that droplet 1 grows faster than droplet 2 over the entire time interval.

Part II: Combating Cryogenic Surface Contamination

4. STATEMENT OF THE PROBLEM

4.1. The Cryogenic Needs of NASA

Large-scale space missions use cryogenic propellants and oxidizers because of their high energy and performance. These systems consume their fuel soon after launch, so current thermal management and insulation systems are adequate and propellant boil-off is acceptable. In contrast, the planned extended-duration, crewed missions will require near-zero boil-off (ZBO) for all systems; otherwise, the required size of a cryogen tank for these missions would be prohibitively large. To realize these missions, NASA has set ambitious goals for high capacity 20 K and 90 K cryocoolers (TA 14.1.2), which will provide cooling to liquid hydrogen and oxygen tanks, respectively.[13] The current state-of-the-art (SOA) cooling capacity for cryocoolers at these operating temperatures, however, are much lower. Furthermore, these next-generation cryocoolers must also be smaller, lighter, and reliable.

4.2. Cryocooler Efficiency Challenges

The low efficiency (≈ 20 %) of cryocoolers results in higher target cooling capacities. Much of the cooling capacity is lost to parasitic heat loads, which can account for over 80 % of the load duty (Figure 4-1), resulting in drastic weight and volume penalties due to oversizing.[14] Two types of parasitic heat loads exist: (1) conductive loads from supports, connections, and cables, and (2) radiative loads from the higher temperature surroundings, which emit in the infrared (IR) spectrum. The parasitic conduction loads are stable and thus predictable over time, while the radiative loads depend on the spectrally dependent emissivity of the cryogenic surface. To combat radiative losses, metallic cryogenic surfaces are plated with a thin layer of smooth gold, which is highly reflective to IR radiation. However, these surfaces are subject to contamination by condensed water-ice

films, which have very high IR absorptivity, gettered from sources on the spacecraft that can increase the IR absorptance in less-predictable ways.

4.3. Counter-Measure to Load Increase

To combat this load increase, the cryogenic system is typically baked to boil off contaminants.[15] However, baking has two drawbacks: (1) the entire cryogenic system is inoperable during decontamination (which can last for days), and by extension whatever instrument it was cooling; (2) deep thermal cycling is stressful and can lead to the mechanical failure of detectors and other cycled components, lowering reliability.[14] Therefore, thermal cycling must be minimized.

4.4. Space Instruments Effected and Outlook

Ice contamination has affected the cryocooler performance of the ISAMS instrument aboard the UARS satellite, the AIRS instrument aboard the Aqua satellite, the MOPITT instrument aboard the EOS Terra satellite, and the OCO-2 instrument aboard the OCO-2 satellite, among others.[14,16-18] Furthermore, contamination is a serious design consideration for the Mid-Infrared Instrument (MIRI) on the James Webb Space Telescope (JWST).[19] Crewed missions will present additional challenges as there will be vastly more water sources that can be gettered onto cryogenic surfaces. Therefore, combating the load increase due to surface contamination is one of the most difficult challenges a cryogenic system designer faces.

4.5. Possible Solution

Due to their low surface energy, hydrophobic surfaces have been shown to delay the nucleation and growth rate of ice from its liquid phase.[20,21] Furthermore, previous studies have demonstrated the spatial control of water nucleation on surfaces patterned with hydrophobic and hydrophilic (high surface energy) regions, known as **biphilic surfaces**.[22,23] The hydrophilic regions serve as preferential nucleation sites, leading to spatial control of where the water nucleates. However,

previous works used non-metallic substrates for either vapor-to-liquid or liquid-to-solid transitions and not the vapor-to-solid (desublimation) transition characteristic of cryocooler contamination. Furthermore, cryocooler operating temperatures (< 100 K) and background pressures (10^{-4} – 10^{-7} Torr) are much lower than those previously investigated. Before discussing the research plan for this project, it is worth expanding more into how a biphilic surface could combat cryogenic surface contamination from an adsorption/desorption standpoint.

4.6. Figures

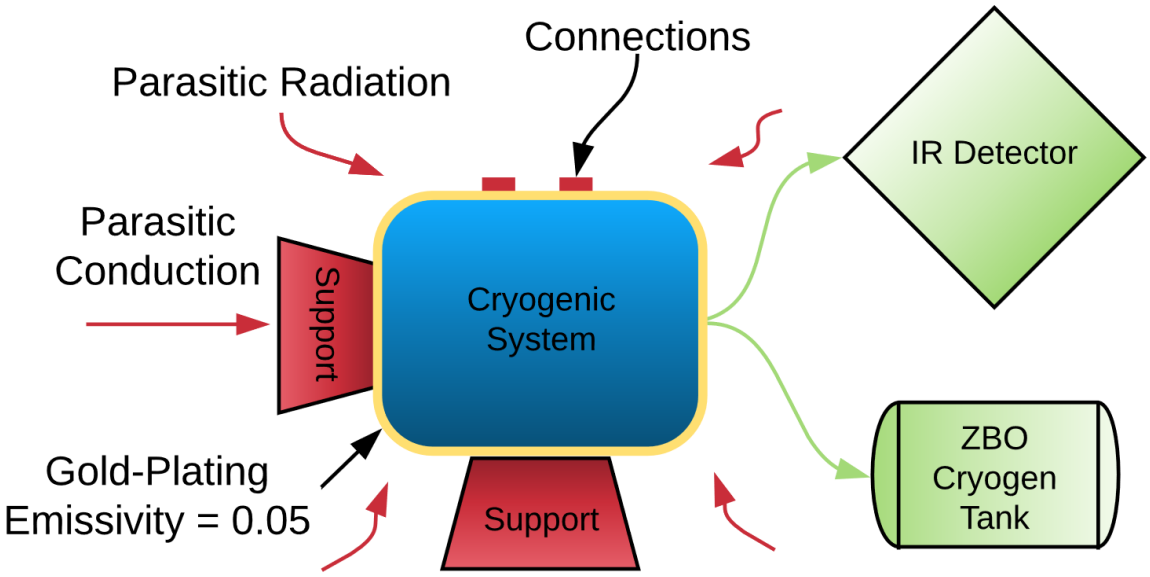

Figure 4-1. *Principal cryocooler loads*. Parasitic loads are red, non-parasitic loads are green.

5. BACKGROUND

5.1. Contamination Physics

Figure 5-1 shows the average amount of time a water molecule spends adsorbed at various interfaces as a function of temperature, capturing how a biphilic surface will resist frost formation. This residence time behavior is governed by the following relation:

$$\tau_r = \tau_o e^{\frac{E_d}{N_o k_B T}} \tag{5-1}$$

where, with appropriate units, τ_r is the residence time, τ_o is the vibrational period between the surface atom and adsorbed molecule, E_d is the desorption energy, N_o is Avogadro's number, k_B is Boltzmann's constant, and T is the temperature of the surface. Note that the only difference between the blue curve (water molecule adsorbed to another water molecule) and the red curve (water molecule adsorbed directly onto a metal surface) is the value of the desorption energy, 40.6 kJ/mol vs 96 kJ/mol.[24] The metal's surface atoms bind stronger with water molecules than water molecules bind with themselves. The desorption energy is essentially the energy required to break the van der Waals bond formed between the surface atom and adsorbed molecule. Note that the residence times are long at cryogenic temperatures, especially for the initial layer adsorbed directly on the surface. Consequently, water molecules that adsorb to cryogenic surfaces never leave—at least not before system baking occurs. However, this is only true because the metal has high surface energy, which results in a high barrier to desorption for the adsorbed molecule.

5.2. Changing the Contamination Physics

The initially adsorbed layer (H_20-metal) forms the tether between the cryogenic surface and subsequent adsorbed layers (H_20-H_20). Therefore, if water molecules can be made to desorb readily from the metal, they will also dislodge the subsequent water layers with them. Water molecules that do not desorb completely will surface diffuse, which is the main purpose of the hydrophilic regions of the biphilic surface—to trap them. Otherwise, a seed ice crystal may nucleate at a random location on the surface and spread in all directions. The hydrophilic regions serve as favorable seed crystal sites and thus serve as favorable frost propagation regions.

5.3. Proposed Change

Desorption energy data was unavailable for water molecules adsorbed to the type of non-polar, hydrophobic thiol compound that I will propose to functionalize the biphilic surfaces with in the next section. However, researchers have found that the binding energy between water molecules and the hydrophobic tails of butanol molecules is 9.65 – 11.58 kJ/mol.[25] Taking 15 kJ/mol as a conservative value for the binding energy between water and the proposed thiol, the dashed black curve in Fig. 2 was plotted. As illustrated by the curve, at a cryogenic temperature of 90 K the average residence time is less than a second for water molecules adsorbed on the hydrophobic regions of the biphilic surface. Since the background vapor pressure is so low, the amount of water molecules incident on the cryogenic surface per unit time is much lower than conventional systems operating around atmospheric pressure. This will inhibit the cluster growth needed for nucleation, thus retarding frost formation. Now that the theory has been established on how biphilic surfaces could combat surface contamination, I now turn to the research plan of this project, including the hypothesis, research questions, objectives and specific aims.

5.4. Figures

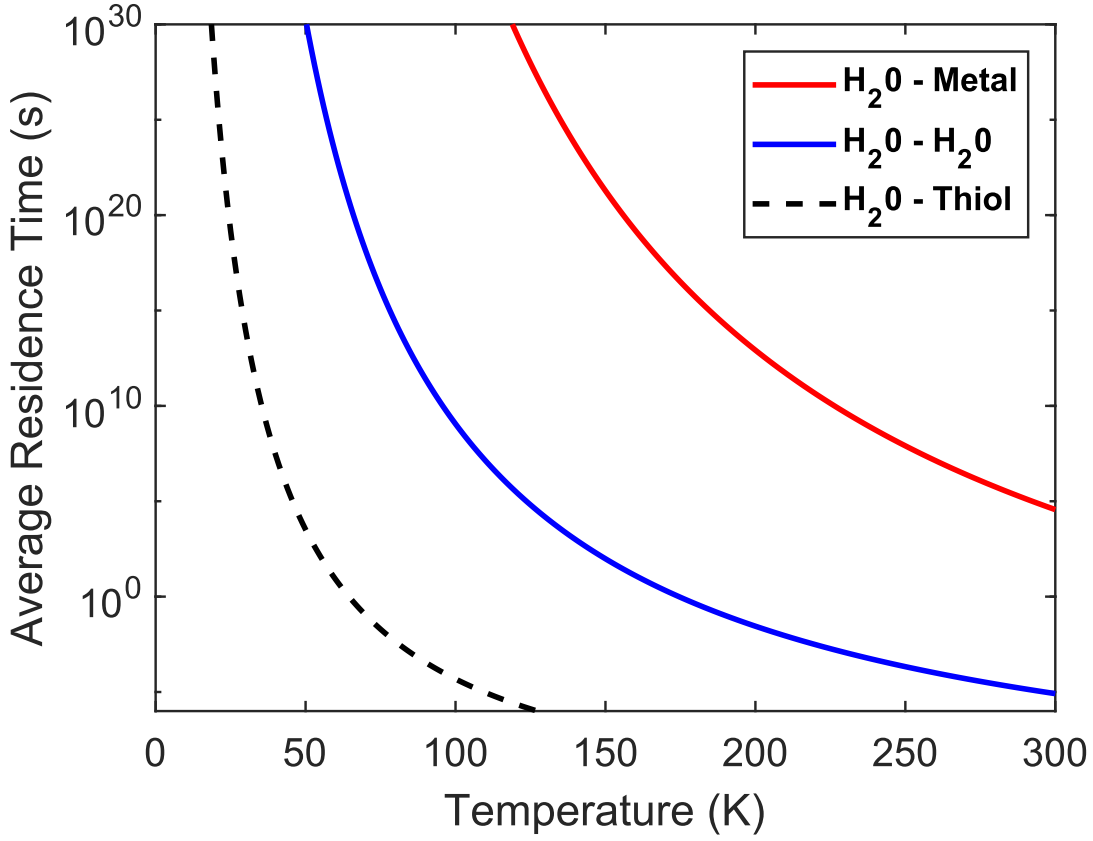

Figure 5-1. *Residence time versus temperature*. Average residence time for water molecules adsorbed at various interfaces.

6. RESEARCH PLAN

6.1. Approach

I propose using a biphilic surface to preferentially nucleate ice on specific areas of the substrate which account for only a fraction (< 5 %) of the overall surface area (Fig. 3.C), effectively serving as on-surface getters. In doing so, the emissivity at the preferential sites will increase, but the overall emissivity of the surface will remain low (Fig. 3.D). Additionally, whereas conventional biphilic surfaces have flat hydrophilic regions, I propose to enhance their performance by using hydrophilic channels instead. At the same projected area as flat surfaces, channels (1) provide more surface area for adsorption/nucleation, (2) have corners which are highly favorable nucleation sites, and (3) have been shown to help confine film growth.[26] As a result, **I hypothesize** that channeled hydrophilic regions will be more effective than flat hydrophilic regions in spatially controlling ice formation. **To assess this** supposed performance enhancement, biphilic surfaces without channels will also be explored in a parallel treatment. Furthermore, I will fabricate a reference gold-plated surface to include in all experiments and characterization for **comparative/assessment** purposes. This project aims to answer the following question:

6.1.1. Research Question

Can a biphilic surface be used to combat surface contamination in space-cryocooler applications? This answer follows from the answers to three related questions:

(1) Does the spatial control of nucleation behavior extend to cryogenic conditions?

(2) Will the biphilic surface maintain the radiation properties of the gold?

(3) Is the biphilic surface robust enough to function over extended periods that include thermal cycling?

Answering the three proceeding questions form the **objectives of this work**. The following **specific aims** will be carried out to meet these objectives.

6.1.2. Aim 1: Fabrication and Characterization of the Biphilic Surfaces

***Fabrication and Surface Functionalization Process with Rationale*.** I will fabricate channeled silicon wafers by lithography and wet etching. In addition to low cost and ease of implementation, wet etching offers great control over the shape, size, and spacing between the channels, which will all govern the film-growth behavior. Due to the corner effect, which results from a high density of dangling bonds where two surfaces meet, channels with sharp (acute) corners better promote nucleation.[26] However, channels with duller corners have higher, ice-accommodating, cross-sectional volume. Therefore, a range of channel shapes will be explored to determine the most effective geometry at controlling contamination in these conditions (Figure 6-1A). Initial channel width and depth will be ≈ 10 μm with a ≈ 200 μm channel spacing as these sizes have been effective in the literature.[26] After creating the channels (omitted for channel-less biphilic surfaces), I will deposit gold using magnetron sputtering, followed by polishing then liquid phase deposition of a hydrophobic, thiol-based, self-assembled monolayer (SAM) to lower the surface energy. I will then remove the thiol from the channels using UV/mask irradiation to expose the underlying, inherently hydrophilic, gold substrate. Non-polar thiols are chosen because they bind well to metals and have been used extensively to functionalize gold.[27] I will explore several thiols to determine which provides the best combination of emittance, frosting performance, and durability.

Rationale for Choosing Silicon. For validation and experimentation, it is desirable to use a fabrication process that allows for quick changes and fine control over the feature geometry. Silicon, having been used for decades in the semiconductor industry, has established protocols and processes that allow for quick, cheap, and effective prototyping of the surface features. Note that the contamination process solely involves the interaction between water and the plated gold layer of the cryogenic surface, not the layer underneath. Therefore, the underlying substrate does not matter for experimental purposes. Once the promising feature geometries are identified, a technique such as laser ablation can be used to fabricate them in aluminum, a typical material used in these applications. Furthermore, by using silicon, the fabrication process steps discussed above to create these surfaces can all be completed in the Micro-Nano-Mechanical Systems (MNMS) cleanroom, here in my home department. This has the advantage of being extremely convenient and that I am well accustomed (see personal statement) to the instruments, protocols, and procedures in this facility, which will facilitate seamless prototyping.

***Characterization with Help from Goddard*.** To verify the functionalization of the biphilic surfaces, water contact angle measurements will be made using a micro-goniometer. The surface structure will be characterized using Scanning Electron Microscopy (SEM) and Atomic Force Microscopy (AFM). Obtaining accurate measurements of surface emittance can be quite challenging due to parasitic heat loads that can skew the results. Here, I will make use of an experimental apparatus that Mike DiPirro (my proposed technical adviser) and other NASA researchers built to measure the emittance properties of JWST's gold-plated stainless steel tubing.[28] A previous study indicates that the absorptance increase from thiol-based SAMs on gold is small (< 3 %).[29] However, this work's measurements were conducted over a narrow range (3-10 μm) of the IR spectrum. Cryogenic surfaces have view factors to bodies that emit at longer (> 10 μm) wavelengths,

necessitating further characterization. I will perform this characterization during my first Center-Based Research Experience (CBRE) at Goddard. Nevertheless, I am not expecting a significant absorptance penalty since the SAM is thin and weakly coupled (relatively speaking) to the internal atomic structure of the gold. Finally, due to their low surface area coverage, I am not expecting a significant absorptance penalty from the channels.

Timeline. I will develop the fabrication and functionalization processes during year one and order all needed supplies (masks, wafers, non-polar thiol compounds, etc.). In-house characterization will start following process development and continue at Goddard during a CBRE.

6.1.3. Aim 2: Frosting/Defrosting Experiments and Model Development

Apparatus. To characterize frost/defrost performance and nucleation studies in conditions encountered by spacecraft cryocoolers, I have designed and am currently building a vacuum system (Figure 6-2). The system can pump down to $\approx 10^{-9}$ Torr, controllably introduce water vapor, and maintain a mounted stage temperature of ≈ 83 K. This system effectively serves as a platform for testing these functionalized surfaces in a relevant environment. I discuss vacuum chamber design considerations in a later chapter.

In-house Experiments. High-speed, high-resolution cameras will be used to capture ice nucleation and growth dynamics from two viewpoints. One camera will capture top-down images of the frost formation on the surface while another camera will capture a side view, allowing for simultaneous imaging of both the spatial control of nucleation exhibited on the biphilic surfaces, as well as the frost layer thickness developed. Using this information, the emission increase and corresponding load increase will be determined from radiation analysis using ice emissivity values based on film thickness (Fig. 3.D). Since the hydrophobic regions of the surfaces will defrost and desorb all water molecules quicker, I will also investigate the defrosting dynamics to determine the optimal

surface properties to minimize cryocooler downtime. Finally, MATLAB will be used to process all images as I have extensive experience with its image processing toolbox from prior work.

Experiments at Goddard. While I can conduct short-term (~ days) experiments using our in-house vacuum system, I cannot conduct the kind of long-term (~ weeks) experiments with large intervals between thermal cycling that characterize actual space-cryocooler applications. Fortunately, I can conduct these experiments during a CBRE at Goddard.

Modeling. Properly sizing a cryocooler requires accurately predicting the expected load increase due to surface contamination. Ultimately, this load increase depends on (1) the fraction of the cryogenic surface that is contaminated, (2) the thickness of the contaminant film, and (3) the emissivity of the contaminant film. The film growth rate is highly sensitive to surface temperature and background vapor pressure, and has been modeled extensively using kinetic theory.[15] However, previous models assume that any molecule that collides with such a cold surface stays adsorbed and fixed indefinitely. The hydrophobic regions of the biphilic surfaces will exert much lower van der Waals forces, which allows molecules to desorb quicker and surface diffuse into the getters, necessitating the development of new models. The models I develop will relate the effect of external conditions (surface temperature and background vapor pressure) and surface properties (surface energy, channel shape, spacing, depth, orientation, etc.) on nucleation behavior (spatial preference and film thickness) to facilitate accurate load increase predictions over time.

Timeline. I will install insulation, camera mounts, an ion gauge, etc., on the vacuum system during the second half of year one. Experiments will begin soon after, followed by model development. Both will continue throughout most of the proposed effort.

6.1.4. Aim 3: Surface Degradation Studies

Methods and Addressing Durability Concerns. Using SEM and AFM, I will investigate the surface degradation mechanisms resulting from continuous operation and thermal cycling and determine how this degradation affects performance. While the durability of these types of coatings is cited as a principal challenge to overcome in technology roadmaps, it is worth noting standard cryocooler operating conditions: typically, they are placed deep within instruments in high vacuum environments where they are not subject to conditions that will seriously compromise performance, such as high temperatures or the shear stresses from fluid flow that are encountered on airplane wings and heat exchangers. Additionally, they are not subject to impact by abrasive particulates that may be encountered on the outside of a spacecraft, for example. Under low-temperature, non-abrasive conditions, these types of functionalized surfaces have shown remarkable durability.[21] Therefore, I am expecting good long-term performance.

Timeline. I will begin degradation studies in year two, following initial experiments, and continue them throughout most of the proposed effort to help identify the best all-around thiol.

6.2. Conclusion

To meet the needs of future NASA space missions, cryocoolers must have higher effective cooling capacities, lower mass/volume, and long reliability. Eliminating the load increase due to contamination of cryogenic surfaces with ice films helps meet all of these performance goals. This proposed work would extend the use of biphilic surfaces down to cryogenic conditions to manipulate the nucleation behavior of water—a non-cryogenic fluid—which has yet to be attempted. The experimental and theoretical knowledge gained could have broad implications to fields in phase change and interfacial phenomena at low temperatures and pressures. If successful,

this project would lay the foundation for an effective approach to combating the load increase due to surface contamination in NASA's space-cryocooler applications.

6.3. Figures

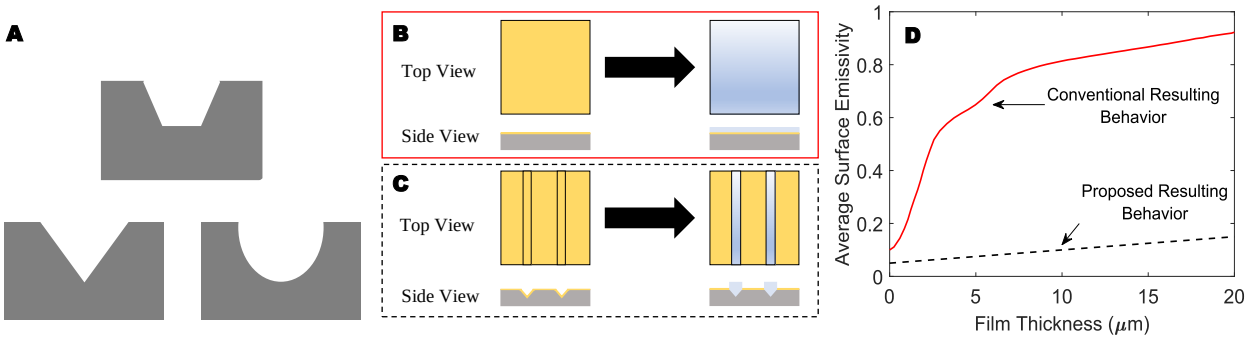

Figure 6-1. *Proposed channel shapes and resulting behavior.* (A) Example channel shapes that will be explored in this work. (B) Uniform ice film grows on bare gold-plated surface. (C) Spatially-controlled, non-uniform ice film grows on functionalized gold-plated surface. The size and spacing between channels have been exaggerated for illustrative purposes. (D) Average surface emissivity to 300 K blackbody radiation as a function of ice film thickness on polished stainless steel at 77 K (solid red curve), adapted from Viehmann et. al (1972). Average surface emissivity as a function of film thickness for proposed functionalized surface (dashed black curve).

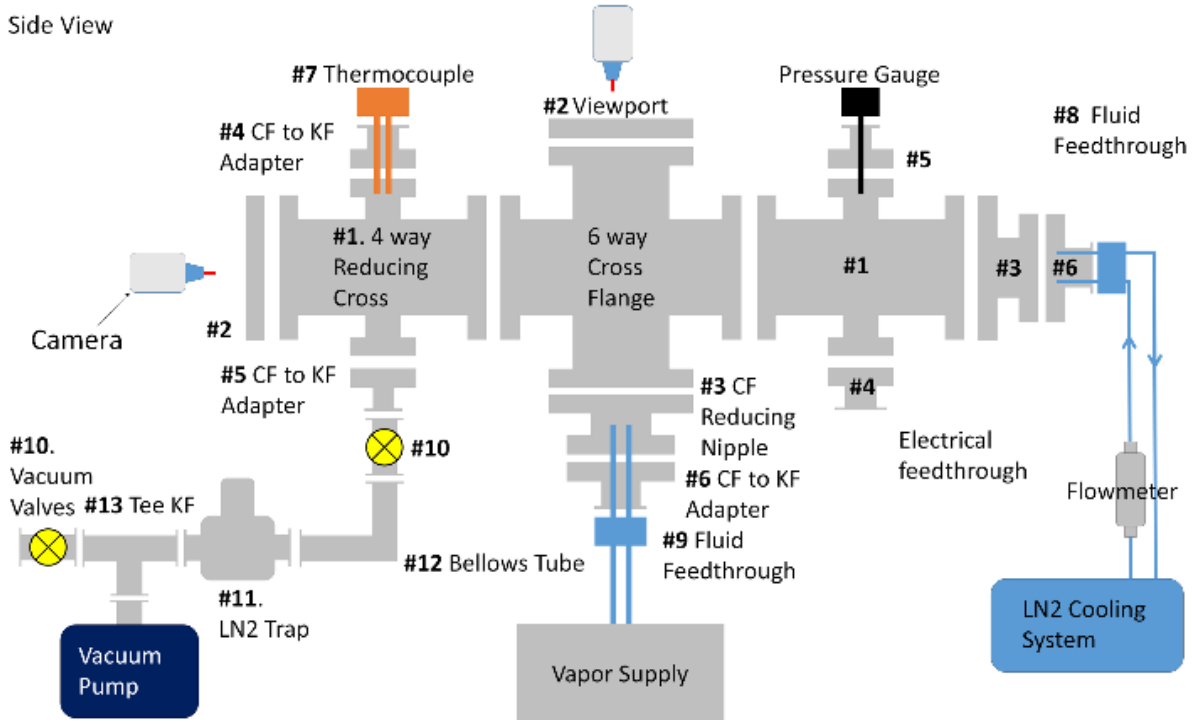

Figure 6-2.*Vacuum chamber schematic.* A side view schematic of the vacuum chamber.

7. VACUUM CHAMBER DESIGN CRITERIA

7.1. Basic Design

Space-cryocooler environments are characterized by high-vacuum pressures ($> 10^{-4}$ Torr) and low temperatures (< 100 K). I designed the chamber to be relatively small to facilitate pump-down to such high vacuum. Pump-down to these levels will require a two-stage pumping system. I will use the roughing pump to pump down to med-high vacuum ($\approx 10^{-3}$ Torr). I will use a turbomolecular pump due to its fast pump-down time and lower maintenance cost when compared to a cryopump. To properly conduct experiments, the vacuum chamber will be fitted with thermocouples, a pressure transducer, various feedthroughs (power, instrumentation, liquid, etc.), insulation, and optics. These components will then be connected to data acquisition software.

7.2. Vapor Supply

To conduct the desublimation frosting experiments, water has to be introduced into the vacuum system. For this purpose, a smaller, vapor-supply chamber was custom ordered from Kurt J. Lesker (Figure 3.2). The chamber consists of an 8in ConFlat full nipple with two 8in flange caps and one 8in viewport. One of the caps was used on the bottom of the full nipple while the other was modified to include five tubes that are 0.5 inches in diameter, four of which being 4 inches long. The fifth tube extends the entire length of the nipple, in addition to extending 4 inches out of the nipple, and is thus 16 inches long. The five tubes are for a liquid fill line, vapor supply line, liquid return line, pressure relief valve, and thermocouple probe. After filling the vapor-supply chamber with deionized water, it will be heated using four 624 W tape heaters, purchased from ETS Equipment Company.

7.3. Heaters

When conducting the desublimation frosting experiments, the chamber walls need to be kept warm so that water vapor does not condense on these surfaces, which could compromise the frosting

experiment. It will also be important to heat the viewports on the chamber as any condensation would decrease visibility during the experiment. To keep the chamber walls warm, I propose using tape heaters that are similar to those proposed for the vapor supply. However, the chamber walls do not need to be nearly as warm as the water in the vapor supply. Therefore, two to three 312 W tape heaters should be more than adequate.

7.4. Viewports

The chamber has four 6in CF flange viewports. Three of the viewports also serve as access doors to the chamber. The viewports are needed for two reasons: (1) for visualization and imaging of the desublimation frosting experiments and (2) to provide enough lighting for the experiments.

REFERENCES.

[1] Zheng, Y. et al., "Directional water collection on wetted spider silk," *Nature* **463(7281)**, (2010).

[2] Parker, A. R. et al., "Water capture by a desert beetle," *Nature* **414(6859)**, (2001).

[3] Wang, Q. et al., "Self-removal of condensed water on the legs of water striders," *Proc Natl Acad Sci U S A* **112(30)**, (2015).

[4] Beér, J. M., "High efficiency electric power generation: The environmental role," *Progress in Energy and Combustion Science* **33(2)**, (2007).

[5] Khawaji, A. D. et al., "Advances in seawater desalination technologies," *Desalination* **221(1-3)**, (2008).

[6] Humplik, T. et al., "Nanostructured materials for water desalination," *Nanotechnology* **22(29)**, (2011).

[7] Peters, T. B. et al., "Design of an Integrated Loop Heat Pipe Air-Cooled Heat Exchanger for High Performance Electronics," *IEEE Transactions on Components, Packaging and Manufacturing Technology* **2(10)**, (2012).

[8] Pérez-Lombard, L. et al., "A review on buildings energy consumption information," *Energy and Buildings* **40(3)**, (2008).

[9] Rose, J. W., "Dropwise condensation theory and experiment: A review," *Proceedings of the Institution of Mechanical Engineers, Part A: Journal of Power and Energy* **216(2)**, (2005).

[10] Rykaczewski, K., "Microdroplet growth mechanism during water condensation on superhydrophobic surfaces," *Langmuir* **28(20)**, (2012).

[11] Rykaczewski, K. et al., "How nanorough is rough enough to make a surface superhydrophobic during water condensation?," *Soft Matter* **8(33)**, (2012).

[12] Yang, Z. et al., "A simple way to fabricate an aluminum sheet with superhydrophobic and self-cleaning properties," *Chinese Physics B* **21(12)**, (2012).

[13] NASA, Technology Roadmaps Area 14: Thermal Management Systems, (2015)

[14] Ross, R. G. in *Spacecraft Thermal Control, Volume 2: Cryogenics* (AIAA, 2002).

[15] Ross, R. G., "Cryocooler Load Increase due to External Contamination of Low-∈ Cryogenic Surfaces," *Cryocoolers 12* (2003).

[16] Ross, R. G., "Performance of the AIRS Pulse Tube Coolers and Instrument—A First Year in Space," *AIP Conference Proceedings* **710(**(2004).

[17] Mand, G. S. et al., "MOPITT On-Orbit Stirling Cycle Cooler Performance," *Cryocoolers* **11(**(2002).

[18] Na-Nakornpanom, A. et al., "In-Flight Performance of the OCO-2 Cryocooler," *IOP Conference Series: Materials Science and Engineering* **101(**(2015).

[19] Ross, R. G., "Estimation of In-Space Emittance (IR absorptance) Increase of MIRI Refrigerant Lines over Time," *Unpublished Work* (2015).
[20] Cao, L. et al., "Anti-Icing Superhydrophobic Coatings," *Langmuir* **25(21)**, (2009).
[21] Wang, Y. et al., "Verification of icephobic/anti-icing properties of a superhydrophobic surface," *ACS Appl Mater Interfaces* **5(8)**, (2013).
[22] Varanasi, K. K. et al., "Spatial control in the heterogeneous nucleation of water," *Applied Physics Letters* **95(9)**, (2009).
[23] Mishchenko, L. et al., "Spatial Control of Condensation and Freezing on Superhydrophobic Surfaces with Hydrophilic Patches," *Advanced Functional Materials* **23(36)**, (2013).
[24] O'Hanlon, J. F. *A User's Guide to Vacuum Technology*. 3rd edn, (2003).
[25] Papagiannakopoulos, P. et al., "Surface Transformations and Water Uptake on Liquid and Solid Butanol near the Melting Temperature," *The Journal of Physical Chemistry C* **117(13)**, (2013).
[26] Lo, C. W. et al., "Control of Ice Formation," *ACS Nano* **11(3)**, (2017).
[27] Pensa, E. et al., "The chemistry of the sulfur-gold interface: in search of a unified model," *Acc Chem Res* **45(8)**, (2012).
[28] Tuttle, J. et al., "Cryogenic thermal absorptance measurements on small-diameter stainless steel tubing," *Cryogenics* **74(**(2016).
[29] Tlili, A. et al., "Adsorption characteristics of self-assembled thiol and dithiol layer on gold," *Materials Science and Engineering: C* **27(4)**, (2007).

APPENDIX A: PHOTOS OF VACUUM CHAMBER

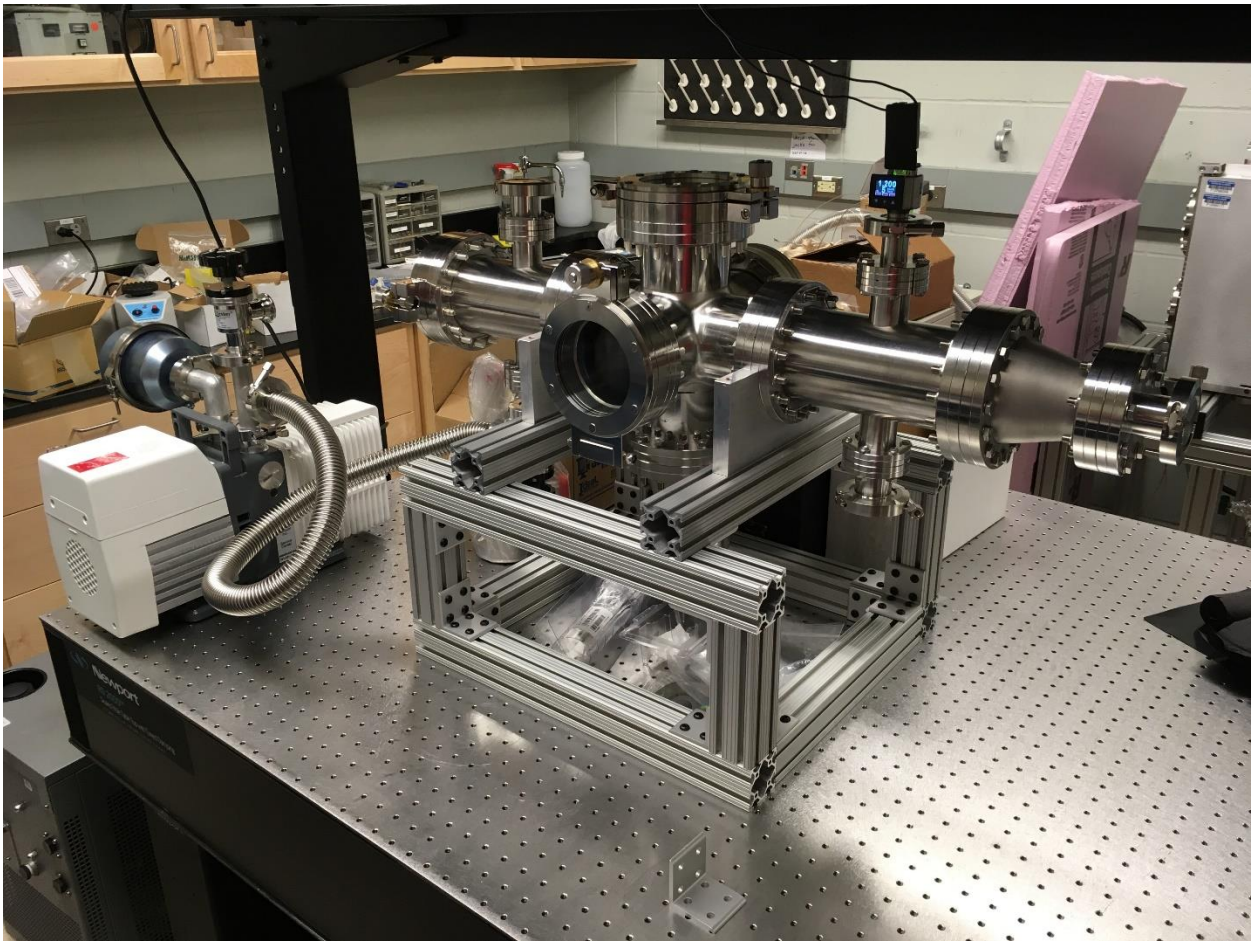

Figure A-1. A photo of the in-progress vacuum system

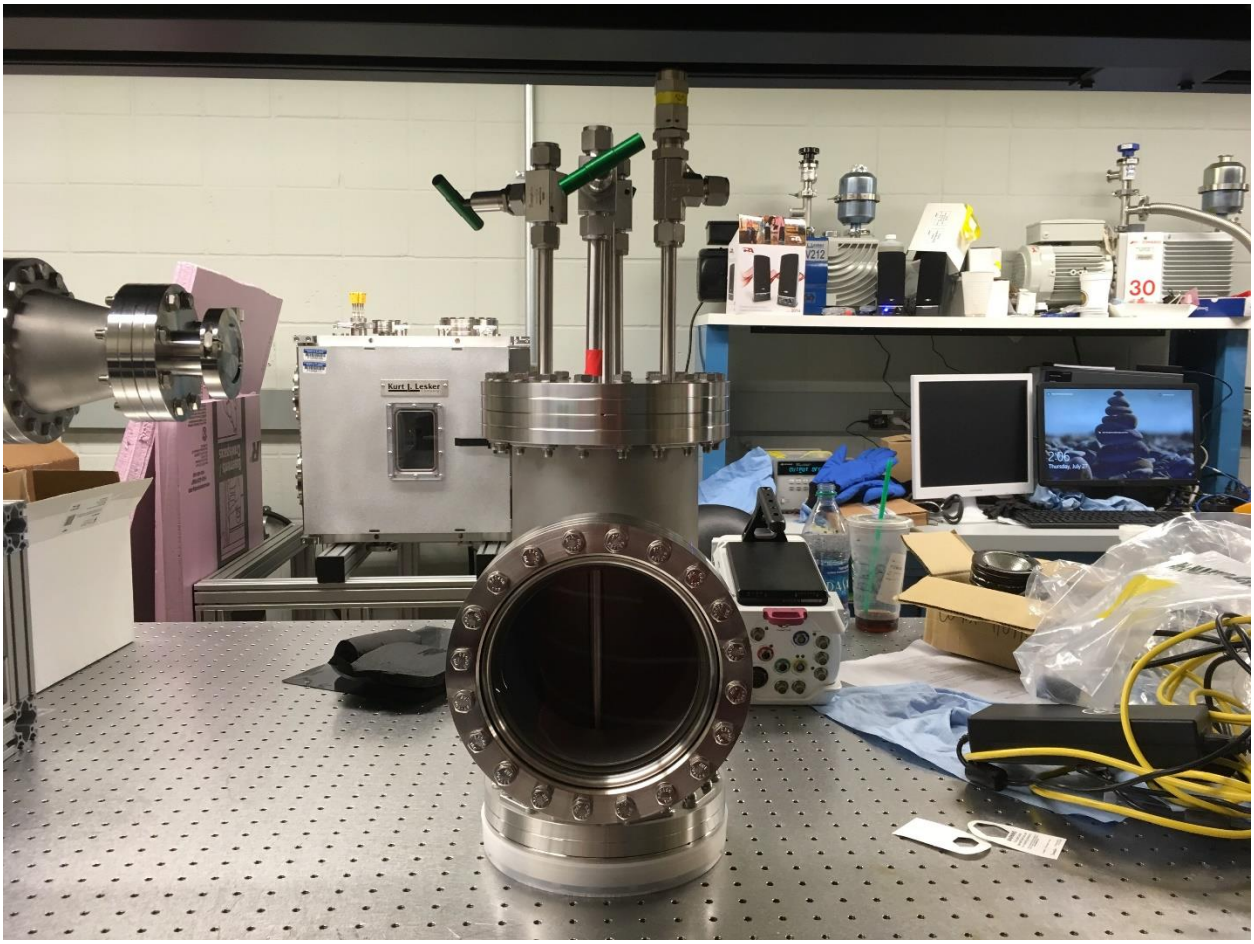

Figure A-2. A Photo of the vapor supply